Simple intrinsic defects in GaAs: Numerical supplement

Peter A. Schultz

Sandia National Laboratories

Simple intrinsic defects in GaAs: Numerical supplement

Peter A. Schultz
Advanced Device Technologies, Dept. 1425
Sandia National Laboratories
P.O. Box 5800
Albuquerque, New Mexico 87185-MS1322

Abstract

This Report presents numerical tables summarizing properties of intrinsic defects in gallium arsenide, GaAs, as computed by density functional theory. This Report serves as a numerical supplement to the results published in: P.A. Schultz and O.A. von Lilienfeld, "Simple intrinsic defects in GaAs", Modelling Simul. Mater. Sci Eng., Vol. **17**, 084007 (2009), and intended for use as reference tables for a defect physics package in device models.

ACKNOWLEDGMENTS

CONTENTS

TABLES

NOMENCLATURE

CBE	conduction band edge
DFT	density functional theory
eV	electron Volt
FDSM	finite defect supercell model
GGA	generalized gradient approximation
IP	ionization potential
LDA	local density approximation
LMCC	local moment countercharge
MSMSE	Modelling and Simulation in Materials Science and Engineering
n/c	not computed
n/x	not exist
PAS09	Article: P.A. Schultz and O.A. von Lilienfeld, MSMSE **17**, 084007 (2009).
PBE	Perdew/Burke/Ernzerhof, a "flavor" of GGA
PP	pseudopotential
SNL	Sandia National Laboratories
VBE	valence band edge

1. INTRODUCTION

The numerical results for density functional theory (DFT) calculations of properties of simple intrinsic defects in gallium arsenide are presented. This condenses the results published in "Simple intrinsic defects in GaAs", P.A. Schultz and O.A. von Lilienfeld (2009), *Modelling and Simulation in Material Science and Engineering*, Vol. 17, Article # 084007 (henceforth "PAS09"). [1] The results of the defect calculations are summarized into a series of numerical Tables containing the parameters needed to populate defect physics packages needed for device simulations. In addition, a summary of the GaAs-specific verification and validation evidence is presented that provides a basis for asserting an overall uncertainty in predicted defect energy levels of the same size as for earlier simulations of silicon defects [2], namely, 0.1-0.2 eV accuracy/uncertainty.

1.1. Computational methods

The details of the computational methods are comprehensive described in PAS09, and will only be briefly summarized here. The DFT calculations were performed with the SEQQUEST code. [3] The defect calculations were performed using both the local density approximation (LDA) [4] and the Perdew-Burke-Ernzerhof (PBE) flavor of the generalized gradient approximation [5], this comparison being a partial assessment of the physical uncertainties within DFT functionals [6]. Calculations with both $3d$-core and $3d$-valence pseudopotentials (PP) were used for the Ga atom, to test (verify) the convergence in the PP construction for defect properties [7]. Augmenting the results described in PAS09, this report adds full defect results for the $3d$-valence PP in the PBE calculations.

The calculations of charged defects used the Finite Defect Supercell Model (FDSM) [2] to incorporate rigorous boundary conditions for the solution of the electrostatic potential in a charged supercell [8] and extrapolate the computed defect energies to the infinitely dilute limit. Defect calculations were performed using 64-atom, 216-atom, and 512-atom cubic supercells. The 216-site supercell calculations proved to be sufficiently converged to achieve the required accuracy and are the default production calculations listed in this Report. Also augmenting the results in PAS09, the calculation of 512-site defect for the LDA simulation context (with a $3d$-core PP for Ga) were extended to all the intrinsic defects done with the 216-site supercells, now including all the interstitials, to provide a comprehensive verification test with respect to supercell size.

These simulation contexts are labeled in the following as: LDA64, LDA, and LDA512, for 64-site, 216-site, and 512-site, respectively, supercell calculations using LDA and the $3d$-core (Z=3) PP for Ga; PBE for the 216-site supercells using PBE and $3d$-core PP; and LDA-3d and PBE-3d for the 216-site supercells with $3d$-valence (Z=13) PP for the Ga atoms.

1.2. Verification and validation

The defect level calculations all used SEQQUEST and the FDSM, the same methods used in DFT calculations of defects in silicon, which yielded mean absolute errors of 0.1 eV and maximum absolute error of 0.2 eV for defect levels over a wide sampling of different defects. This is the expected accuracy (uncertainties) of the methods for defect level calculations in GaAs, and the limit of the physical accuracy of the DFT approximations used in this analysis.

The pseudopotentials used in the GaAs calculation, as described in PAS09, were extensively verified in Ref. [7], and validated for the bulk crystalline calculations. The PP used in this study were further tested here, all defect calculations were performed with both the 3*d*-core and 3*d*-valence PP for Ga. While absolute formation energies differed by as much as 0.4 eV (for the gallium antisite, Ga_{As}), the differences were typically much smaller. The defect level results differed with PP by at most 0.11 eV, indicated an effective cancellation of errors was occurring. Hence, uncertainties in the absolute formation energies might be as large as 0.4 eV, but the (3*d*-core) defect levels, obtained as differences in formation energies, have much smaller uncertainties, of 0.1 eV, with respect to pseudopotential construction. The bulk properties obtained for GaAs with these simulation contexts are in the following Table.

Table 1. Computed bulk GaAs properties

Simulation context	Lattice parameter (Å)	Bulk Modulus (GPa)	Kohn-Sham Band gap (eV)	Formation energy (eV)
Experiment	5.65 (a)	79 (a)	1.52 (b)	0.74 (c)
LDA	5.599	72.4	0.83	0.787
LDA-3d	5.628	77.0	0.47	0.636
PBE	5.739	59.6	0.45	0.824
PBE-3d	5.767	59.9	0.13	0.694

(a) Ref. [9].
(b) Ref. [10].
(c) Ref. [11].

The good comparisons between the results for neutral defect formation energies obtained with SEQQUEST (comparisons unaffected by the idiosyncracies of treating charged supercells) and other calculations with other methods, with different basis sets and difference pseudopotentials, as described in PAS09, provide additional verification of the basis sets and PP used in these calculations.

The comparison of GaAs defect results with different functionals, LDA vs. PBE, indicates a larger uncertainty due to the physical approximation of DFT. While mostly qualitatively the same, the numerical differences in LDA and PBE computed defect levels are as large as 0.3 eV. Results for silicon defects indicated that PBE are more reliable (lower maximum errors) for -*U* transitions involving structural rearrangements. The GaAs defects are predicted to have multiple -*U* transitions and structural rearrangements, suggesting that PBE might be necessary to achieve the 0.1-0.2 eV target accuracy seen in computations of defect levels in silicon.

1.2.1. Extrapolation model

The total energy calculations for the charged defects used a modified-Jost model [12,2] to evaluate the missing charge polarization (screening) energy outside the finite volume of the supercell:

$$E_{pol} = (1 - 1/\varepsilon_0) \, q^2/R_{Jost} \tag{1}$$

where ε_0 is the static dielectric constant, and $R_{Jost} = (R_{sphere}-R_{skin})$ is the radius of a sphere with a volume equal to the volume of the supercell, R_{sphere}, less the skin depth, R_{skin}, of an unscreened surface region within the sphere. R_{skin} must be calibrated (fit) once for each material system.

The *extrapolation model* was *calibrated* via calculations of negative charge states of the gallium vacancy, in unrelaxed tetrahedral structures for the (1-), (2-), and (3-) charge states, and then pre-verified using fully relaxed arsenic antisite (0/1+) and (1+/2+) charge transitions.

The *extrapolation model* was comprehensively *verified* via comparisons of defect calculations extrapolated to infinitely dilute defects from 64-site, from 216-site, and from 512-site supercell calculations. 216-site cells were assessed to be necessary to meet required level of quantitative confidence. The complete set of extrapolated defect calculations with 216-site supercells were repeated using 512-site supercells. The largest difference in any defect level was 0.05 eV, mostly much smaller, indicating uncertainty with respect to cell size (and k-point sampling) is less than 0.05 eV.

The *extrapolation model* was *validated*. The experimental GaAs dielectric constant, 13.0, for ε_0 and a physically reasonable unpolarized "skin depth" (R_{skin}), 1.6 bohr, led to a converged extrapolation, and these parameters are also consistent with extrapolation models in multiple other III-V defect calculations such as AlAs, InP, and GaP (experimental ε_0 and $R_{skin}=1.5(2)$)

The quantities defining the extrapolation model are summarized in the next Table.

Table 2. Supercell extrapolation energies, ε_0=13.0, R_{skin}=1.6 bohr.

Context:	LDA64	LDA512	LDA	LDA-3d	PBE	PBE-3d
a_0(Å)	5.599	5.599	5.599	5.628	5.739	5.767
IP(VBE) (eV)	5.31	5.48	5.40	5.40	5.15	5.19
Charge	External polarization energy (eV), Eq. 1					
|q| = 1	1.0895	0.5094	0.6942	0.6903	0.6758	0.6723
|q| = 2	4.3579	2.0375	2.7768	2.7612	2.7031	2.6891
|q| = 3	9.8052	4.5844	6.2477	6.2126	6.0819	6.0504
|q| = 4	17.4314	8.1501	11.1071	11.0446	10.8124	10.7563

1.2.2. Validation of GaAs defect results

The amount of data available to quantitatively validate GaAs defect results is miniscule in comparison to silicon. The goal is to identify as many points of validation as possible, and determine if the comparisons are consistent with the magnitude of uncertainties found, using the same methods, in silicon. The GaAs defect results were validated against (1) *EL*2 vs. aAs properties: defects levels, and barrier to return; (2) reproducing the band gap with the span of the computed defect level spectrum; (3) positions of the *E*1 and *E*2, and *E*3 defect levels with the newly re-assigned vv(4-/3-) and vv(3-/2-) transitions and the $-U$ v_{As}(3-/1-) transition; and (4) the inferred *p*-type thermal migration barrier for the arsenic interstitial. In each case, the quantity inferred from experiment and the value from the simulation is within 0.1 eV, consistent with the Si assessed overall uncertainty of 0.1-0.2 eV.

This page intentionally left blank

2. RESULTS

The section contains the Tables that summarize the numerical results for DFT simulations of defects in GaAs.

2.1. Defect atomic structures

The following Tables list the ground state structures for the simple intrinsic defects in GaAs as a function of charge state. The bonding structures are all illustrated in PAS09. In the vacancies, note the discriminating nomenclature: v' refers to the simple vacancy, and v^* refers to the site-shifted form of the vacancy (where a nearest-atom to the vacancy hops into the vacant site, thus creating a vacancy-antisite pair).

Table 3. Ground state structure designations for vacancy and antisite defects.

Charge state	$v' = v_{Ga}$ $v^*=v_{As}As_{Ga}$	$v' = v_{As}$ $v^*=v_{Ga}Ga_{As}$	vv	aAs	aGa (T_d)[a]
(4-)	-	-	C_{1h}-pair(Ga)	-	-
(3-)	v'/T_d	v^*/C_{3v}	C_{1h}-pair(Ga)	-	-
(2-)	$v'/\sim T_d$	v^*/C_{3v}	C_{1h}-pair(Ga)	-	T_d
(1-)	$v'/\sim T_d$	v'/pair-D_{2d}	C_{1h}-pair(Ga)	-	$\sim T_d$ (res-D_{2d})
(0)	$v'/\sim T_d$	v'/pair-D_{2d}	C_{3v}-out(Ga)	T_d	$\sim T_d$ (res-D_{2d})
(1+)	v^*/C_{1h}-pair(Ga)	v'/pair-C_{2v}	$\sim C_{3v}$-out(Ga)	T_d	$\sim T_d$ (res-D_{2d})
(2+)	v^*/C_{1h}-pair(Ga) v^*/C_{3v}-out{pbe3d}	v'/T_d-out(Ga)	$\sim C_{3v}$-out(Ga)	T_d	T_d
(3+)	v^*/C_{3v}-out(Ga)	v'/T_d-out(Ga)	-	-	-

(a) Results for the Ga antisite presented here are all constrained to T_d. The gallium antisite is Jahn-Teller unstable, and in the (1-), (0), (1+) charge states distorts to D_{2d}, but the largest energy lowering is 0.05 eV, and is ignored in the following.

Table 4. Ground state structure designations for the interstitials and di-antisite.

Charge state	Ga_i	As_i	aa[a]
(1-)	C_{2v} split-(110)$_{Ga}$	[b]C_2-twisted split-110$_{As}$	-
(0)	C_{2v} split-(110)$_{Ga}$	C_{2v} split-110$_{As}$	C_{3v}
(1+)	$T_{i,Ga}$	C_{1h} p-(001)$_{Ga}$	-
(2+)	$T_{i,As}$	C_{3v} H —or— C_{1h} B_g {lda,pbe}	-
(3+)	$T_{i,As}$	$T_{i,Ga}$ {lda} —or— $T_{i,As}$ {pbe}	-

(a) Only the results for high-symmetry C_{3v} di-antisite structures are presented. The symmetry-reducing distortions (to C_{1h}) give negligible energy lowering.

(b) The C_2 twisted form of the split-110$_{As}$ had not been discovered at the time PAS09 was published. The lowering from the C_{2v} split-110$_{As}$ is negligible (<0.01 eV) for the 3d-core LDA contexts, but is 0.05 for the LDA-3d and PBE and 0.10 for PBE-3d context, and therefore merits updating.

2.2. Defect charge transition energy levels

This section presents the defect charge transition levels of the simple intrinsic defects in GaAs, in eV, along with neutral formation energies. The defect level calculations are the primary result of the Report, the later formation energies are all derived from these results.

Table 5. Defect levels for the gallium vacancy, in eV, referenced to the VBE:
V_{Ga} (v') ⬚ v_{As}-As_{Ga} (v*)

V_{Ga} Context	Neutral formation energy	Defect levels (eV), cf. VBE						
		(3+/2+)	(2+/1+)	(1+/0)	(0/1-)	(1-/2-)	(2-/3-)	(3-/4-)
Unrelaxed T_d-v' (for polarization calibration)								
LDA64	3.167	n/c	n/c	n/c	0.527	0.841	1.181	n/x
LDA	3.244	n/c	n/c	n/c	0.609	0.890	1.230	n/x
LDA512	3.327	n/c	n/c	n/c	0.596	0.871	1.211	n/x
Relaxed thermodynamic levels								
LDA64	2.81	n/c	n/c	n/c	0.34	0.52	0.68	n/x
LDA512	2.75	0.16	0.14	0.39	0.48	0.62	0.79	n/x
LDA	2.69	0.27	0.06	0.34	0.48	0.64	0.80	n/x
LDA-3d	2.50	0.24	-0.03	0.40	0.53	0.67	0.81	n/x
PBE	2.65	0.63	0.11	0.60	0.49	0.65	0.81	n/x
PBE-3d	2.48	0.62	0.15	0.51	0.52	0.66	0.81	n/x

Table 6. Defect levels for the arsenic vacancy, in eV, referenced to the VBE:
V_{As} (v') ⬚ v_{Ga}-Ga_{As} (v*)
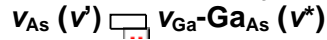
V_{As} Context	Neutral formation energy	Defect levels (eV), cf. VBE						
		(3+/2+)	(2+/1+)	(1+/0)	(0/1-)	(1-/2-)	(2-/3-)	(3-/4-)
LDA512	3.54	0.30	-0.16	0.90	0.57	1.46	0.95	n/x
LDA	3.55	0.25	-0.18	0.91	0.57	1.42	0.96	n/x
LDA-3d	3.41	0.30	-0.16	0.87	0.55	1.29	0.94	n/x
PBE	3.44	0.51	0.05	1.06	0.67	1.38	0.93	n/x
PBE-3d	3.30	0.55	0.06	1.02	0.66	1.23	0.91	n/x

Table 7. Defect levels for the divacancy, in eV, referenced to the VBE:
$$vv = v_{As} \text{---} v_{Ga}$$

vv Context	Neutral formation energy	Defect levels (eV), cf. VBE						
		(3+/2+)	(2+/1+)	(1+/0)	(0/1-)	(1-/2-)	(2-/3-)	(3-/4-)
LDA512	4.21	n/x	0.15	0.28	0.72	0.58	1.51	1.53
LDA	4.19	n/x	0.15	0.28	0.72	0.58	1.48	1.50
LDA-3d	4.05	n/x	0.20	0.30	0.73	0.60	1.43	1.43
PBE	3.59	n/x	0.18	0.30	1.09	0.59	1.55	1.50
PBE-3d	3.44	n/x	0.21	0.31	1.10	0.60	1.49	1.42

Table 8. Defect levels for the arsenic antisite, in eV, referenced to the VBE:
$$aAs = As_{Ga}$$

As_{Ga} Context	Neutral formation energy	Defect level (eV), cf. VBE						
		(3+/2+)	(2+/1+)	(1+/0)	(0/1-)	(1-/2-)	(2-/3-)	(3-/4-)
LDA64	1.53	n/x	0.50	0.74	n/x			
LDA512	1.51	n/x	0.48	0.73	n/x			
LDA	1.50	n/x	0.48	0.73	n/x			
LDA-3d	1.48	n/x	0.50	0.73	n/x			
PBE	1.27	n/x	0.50	0.73	n/x			
PBE-3d	1.24	n/x	0.51	0.73	n/x			

Table 9. Defect levels for the gallium antisite, in eV, referenced to the VBE:
$$aGa = Ga_{As}$$

[a]Ga_{As} (T_d) Context	Neutral formation energy	Defect level (eV), cf. VBE						
		(4+/3+)	(3+/2+)	(2+/1+)	(1+/0)	(0/1-)	(1-/2-)	(2-/3-)
LDA512	3.24	-	-	0.26	0.39	0.55	0.74	n/x
LDA	3.19	-	-	0.26	0.40	0.57	0.77	n/x
LDA-3d	2.80	-	-	0.32	0.45	0.60	0.78	n/x
PBE	3.20	-	-	0.29	0.44	0.60	0.78	n/x
PBE-3d	2.85	-	-	0.33	0.46	0.61	0.77	n/x

(a) The gallium antisite results presented here are for a symmetric T_d configuration. The middle charges undergo small distortions, less than 0.05 eV, and these are ignored here.

Table 10. Defect levels for the di-antisite, in eV, referenced to the VBE:
$$aa = Ga_{As}\text{—}As_{Ga}$$

aa Context	Neutral formation energy	Defect levels (eV), cf. VBE						
		(4+/3+)	(3+/2+)	(2+/1+)	(1+/0)	(0/1-)	(1-/2-)	(2-/3-)
LDA512	2.53	-	-	-	-	-	-	-
LDA	2.52	-	-	-	-	-	-	-
LDA-3d	2.26	-	-	-	-	-	-	-
PBE	2.44	-	-	-	-	-	-	-
PBE-3d	2.19	-	-	-	-	-	-	-

Table 11. Defect levels for the gallium interstitial, in eV, referenced to the VBE: iGa = Ga$_i$

Ga$_i$ Context	Neutral formation energy[a]	Defect levels (eV), cf. VBE						
		(3+/2+)	(2+/1+)[b] ($T_{i,Ga}$[+])	(1+/0)[b] ($T_{i,Ga}$[+])	(0/1-)	(3+/2+)	(2+/1+)[c] ($T_{i,As}$[+])	(1+/0)[c] ($T_{i,As}$[+])
LDA512	(4.25)	0.04	-0.02	1.98	-	0.04	0.24	1.72
LDA	(4.26)	0.05	-0.02	2.00	-	0.05	0.25	1.72
LDA-3d	(4.10)	0.00	-0.03	1.99	-	0.00	0.18	1.78
PBE	(4.20)	0.14	0.12	2.02	-	0.14	0.30	1.83
PBE-3d	(4.02)	0.08	0.08	2.00	-	0.08	0.23	1.85

(a) Note that Ga$_i$(0) is thermodynamically unstable to e- emission to Ga$_i$(1+) .
(b) Thermodynamic levels traversing charge state ground states: $T_{i,Ga}(1+)$–$T_{i,As}(2+)$–$T_{i,As}(3+)$.
(c) Levels of the Ga$_i$ trapped in the $T_{i,As}$ site (i.e., excluded from $T_{i,Ga}(1+)$ ground state).

Table 12. Defect levels for the arsenic interstitial, in eV, referenced to the VBE: iAs = As$_i$

As$_i$ Context	Neutral formation energy	Defect levels (eV), cf. VBE						
		(3+/2+)	(2+/1+)	(1+/0)	(0/1-)	(1-/2-)	(2-/3-)	(3-/4-)
LDA512	3.56	0.35	-0.30	0.93	0.83	n/x		
LDA	3.58	0.36	-0.25	0.93	0.84	n/x		
LDA-3d	3.51	0.33	-0.16	0.90	0.86	n/x		
PBE	3.46	0.38	-0.23	1.07	0.88	n/x		
PBE-3d	3.38	0.30	-0.04	0.96	0.96	n/x		

2.3. Defect formation energies

The ground state defect formation energies, as a function of charge state are trivially obtained by simple arithmetic from the neutral formation energies and the computed defect charge transition energy levels in the previous section. As all the results in this Report, the defect formation energies in these Tables are presented in the arsenic-rich limit. The formation energies of the charged defects are presented with the Fermi level at the VBE. The Tables present the formation energies of all the simple intrinsic defects, segregated by simulation context.

The gallium interstitial quotes two formation energies for the (+) charge, the first is the ground state of the (+) state in the non-bond tetrahedral interstitial site with Ga nearest neighbors: $T_{i,Ga}$. This configuration does not have any other stable charge states in the DFT calculation (the Kohn-Sham eigenstate dips below the valence band states, and, therefore, the local (2+) and (3+) defect states cannot be accurately computed). The $T_{i,As}$ has charge states from (1+) through (3+), and is the ground state for the (2+) and (3+), and therefore its formation energy is also quoted.

Table 13. Formation energies of GaAs defects at VBE, in eV, context = LDA512.

Charge state	vGa	vAs	*vv*	aAs	aGa (T_d)	*aa*	iGa $T_{i,Ga}$; $T_{i,As}$	iAs
(4-)	-	-	8.55	-	-	-	-	-
(3-)	4.64	6.52	7.02	-	-	-	-	-
(2-)	3.85	5.57	5.51	-	4.53	-	-	-
(1-)	3.23	4.11	4.93	-	3.79	-	-	4.39
(0)	**2.75**	**3.54**	**4.21**	**1.51**	**3.24**	**2.53**	**(4.25)**	**3.56**
(1+)	2.36	2.64	3.93	0.78	2.85	-	2.27;2.53	2.63
(2+)	2.22	2.80	3.78	0.30	2.59	-	2.29	2.93
(3+)	2.06	2.50	-	-	-	-	2.25	2.58

Table 14. Formation energies of GaAs defects at VBE, in eV, context = LDA.

Charge state	vGa	vAs	*vv*	aAs	aGa (T_d)	*aa*	iGa $T_{i,Ga}$; $T_{i,As}$	iAs
(4-)	-	-	8.47	-	-	-	-	-
(3-)	4.61	6.50	6.97	-	-	-	-	-
(2-)	3.81	5.54	5.49	-	4.53	-	-	-
(1-)	3.17	4.12	4.91	-	3.76	-	-	4.42
(0)	**2.69**	**3.55**	**4.19**	**1.50**	**3.19**	**2.52**	**(4.26)**	**3.58**
(1+)	2.35	2.64	3.91	0.77	2.79	-	2.26;2.54	2.65
(2+)	2.29	2.82	3.76	0.29	2.53	-	2.29	2.90
(3+)	2.02	2.57	-	-	-	-	2.24	2.54

Table 15. Formation energies of GaAs defects at VBE, in eV, context = LDA-3d.

Charge state	vGa	vAs	*vv*	aAs	aGa (T_d)	*aa*	iGa $T_{i,Ga}$; $T_{i,As}$	iAs
(4-)	-	-	8.24	-	-	-	-	-
(3-)	4.51	6.19	6.81	-	-	-	-	-
(2-)	3.70	5.25	5.38	-	4.18	-	-	-
(1-)	3.03	3.96	4.78	-	3.40	-	-	4.37
(0)	**2.50**	**3.41**	**4.05**	**1.48**	**2.80**	**2.26**	**(4.10)**	**3.51**
(1+)	2.10	2.54	3.75	0.75	2.35	-	2.11;2.32	2.61
(2+)	2.13	2.70	3.55	0.25	2.03	-	2.14	2.77
(3+)	1.89	2.40	-	-	-	-	2.14	2.44

Table 16. Formation energies of GaAs defects at VBE, in eV, context = PBE.

Charge state	vGa	vAs	*vv*	aAs	aGa (T_d)	*aa*	iGa $T_{i,Ga}$; $T_{i,As}$	iAs
(4-)	-	-	8.32	-	-	-	-	-
(3-)	4.60	6.42	6.82	-	-	-	-	-
(2-)	3.79	5.49	5.27	-	4.58	-	-	-
(1-)	3.14	4.11	4.68	-	3.80	-	-	4.34
(0)	**2.65**	**3.44**	**3.59**	**1.27**	**3.20**	**2.44**	**(4.20)**	**3.46**
(1+)	2.05	2.38	3.29	0.54	2.76	-	2.18;2.37	2.39
(2+)	1.94	2.33	3.11	0.04	2.47	-	2.07	2.62
(3+)	1.31	1.82	-	-	-	-	1.93	2.24

Table 17. Formation energies of GaAs defects at VBE, in eV, context = PBE-3d.

Charge state	vGa	vAs	*vv*	aAs	aGa (T_d)	*aa*	iGa $T_{i,Ga}$; $T_{i,As}$	iAs
(4-)	-	-	8.05	-	-	-	-	-
(3-)	4.47	6.10	6.63	-	-	-	-	-
(2-)	3.66	5.19	5.14	-	4.23	-	-	-
(1-)	3.00	3.96	4.54	-	3.46	-	-	4.34
(0)	**2.48**	**3.30**	**3.44**	**1.24**	**2.85**	**2.19**	**(4.02)**	**3.38**
(1+)	1.97	2.28	3.13	0.51	2.39	-	2.02;2.17	2.42
(2+)	1.82	2.22	2.92	0.00	2.06	-	1.94	2.46
(3+)	1.20	1.67	-	-	-	-	1.86	2.16

2.4. Defect migration energies

Only two intrinsic defects are potentially mobile: the Ga_i and As_i. All other defects will be immobile at room or operating temperature (certainly for the time scales of interest for radiation damage). In addition to potential thermal diffusion, the As_i is predicted to exhibit athermal diffusion [13] (via carrier-driven Bourgoin-Corbett diffusion [14]) in *p*-type GaAs, and potentially recombination-enhanced diffusion in *n*-type GaAs.

2.4.1. Gallium interstitial – thermal diffusion

The Ga interstitial has limited number of accessible structures and charge states, with the DFT calculations only finding thermodynamically stable states for the (1+), (2+), and (3+) charge states, and the non-bonded tetrahedral interstitial positions being strongly favored against all other structures. The gallium interstitial can potentially migrate thermally, through either the hexagonal site (via a $T_{i,As}$—H—$T_{i,Ga}$—H—$T_{i,As}$ path) or through a split-(110)$_{Ga}$ site (via a kick-out mechanism). The lower energy hexagonal path cannot be fully characterized for the (2+) and (3+) charge states, as the defect Kohn-Sham eigenstate dips below the VBE for the $T_{i,Ga}(2+;3+)$ and a rigorous defect energy cannot be computed with current methods, but it can be unambiguously identified as a local minimum basin through which the interstitial could traverse. In AlAs, this entire path remains clear of the VBE, suggesting a similar path is viable here.

Table 18. Diffusion barriers (thermal) for the gallium interstitial, in eV.

Pathway:	Hexagonal site (*H*)			Split-(110)$_{Ga}$ site		
Context	$Ga_i(1+)$	$Ga_i(2+)$	$Ga_i(3+)$	$Ga_i(1+)$	$Ga_i(2+)$	$Ga_i(3+)$
LDA512	1.22	0.82	0.67	1.10	0.92	>[0.93]
LDA	1.22	0.79	0.63	1.12	0.94	1.00
LDA-3d	1.18	0.78	0.58	1.14	0.94	0.92
PBE	1.11	0.76	0.63	1.07	0.93	0.97
PBE-3d	1.07	0.74	0.60	1.09	0.92	0.90

2.4.2. Arsenic interstitial – thermal diffusion

Migration paths and barriers for the As interstitial were only obtained for *p*-type GaAs, an incidental byproduct of a comprehensive search for ground state structures. The thermal barrier for migration for the $As_i(3+)$ migration is 0.3-0.4 eV via a non-bonded $T_{i,As}$—H—$T_{i,Ga}$ pathway, the hexagonal (*H*) site being the saddle point between the lower-energy *T* sites. The thermal barrier for $As_i(2+)$ is also 0.3-0.4 eV, along the same pathway, except that the *H*-site is the ground state, and the *T*-sites are the barriers. Evaluating the thermal barrier for $As_i(3+)$ is complicated for the LDA, by the *H*-site descending (very slightly) into the VBE. The data in brackets in the following Table indicates energies that are likely slightly (<0.1eV) underestimated, as this is the self-consistent calculation of the delocalized state embedded in the VBE rather than the localized defect state it is almost degenerate with. The thermal migration barrier agrees with a value, 0.5 eV, inferred from extensive experimental data [15].

Table 19. Diffusion barriers (thermal) for the arsenic interstitial, in eV.

Context		As$_i$(2+) 0.4 eV			As$_i$(3+) 0.4 eV(LDA), 0.3 eV(PBE)		
	B_g	$T_{i,As}$ (barrier)	H	$T_{i,Ga}$	$T_{i,As}$	$H^{(a)}$ (barrier)	$T_{i,Ga}$
LDA512	vb	+0.41	0	+0.23	+0.09	>[+0.32]	0
LDA	-0.01	+0.40	0	+0.18	+0.10	+0.44	0
LDA-3d	+0.08	+0.36	0	+0.20	+0.12	>[+0.26]	0
PBE	-0.02	+0.38	0	+0.26	0	+0.34	+0.04
PBE-3d	+0.18	+0.43	0	+0.35	0	+0.27	+0.09

(a) The values in brackets are approximate; the calculated state is a mixed delocalized-defect state where the defect eigenstate has dipped into the VBE.

2.4.3. Athermal and recombination enhanced diffusion: arsenic interstitial

The arsenic interstitial will diffuse athermally in *p*-type. One Bourgoin-Corbett migration path emerges from the search for ground state structures, diffusion driven by capture of carriers:

$$T_{i,As}(3+) \longrightarrow H(2+) \longrightarrow T_{i,Ga}(3+) \longrightarrow H(2+) \longrightarrow \ldots$$
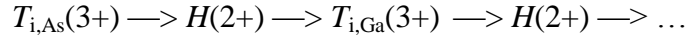
as the tetrahedral interstitial ground state captures an electron and collapses downhill, without a barrier, to the *H* site, which, in turn, re-emits the electron, and collapses downhill, without a barrier back into a *T* site. There are further paths that capture yet more electrons and then insert into the lattice, and then re-emerge into different *T* site upon re-emitting their electrons. The relatively flat landscape and multiple bistabilities and changes in structure for the (1-), (0), and (1+) charge states further suggest that recombination enhanced diffusion is likely among these charge states of the arsenic interstitial.

3. CONCLUSIONS

The parameters needed to describe the defect properties of simple intrinsic defects in GaAs are summarized into Tables, tabulating the numerical results presented in PAS09.

4. REFERENCES

1. P.A. Schultz and O.A. von Lilienfeld, Modelling Simul. Mater. Sci. Eng. **17**, 084007 (2009).
2. P.A. Schultz, Phys. Rev. Lett. **96**, 246401 (2006).
3. SEQQUEST code, unpublished, http://dft.sandia.gov/quest/
4. J.P. Perdew and A. Zunger, Phys. Rev. **23**, 5048 (1981).
5. J.P. Perdew, K. Burke, and M. Ernzerhof, Phys. Rev. Lett. **77**, 3865 (1996).
6. A.E. Mattsson, P.A. Schultz, M.P. Desjarlais, T.R. Mattsson, and K. Leung, Modelling Simul. Mater. Sci. Eng. **13**, R1 (2005).
7. O.A. von Lilienfeld and P.A. Schultz, Phys. Rev. B **77**, 115202 (2008).
8. P.A. Schultz, Phys. Rev. B **60**, 1551 (1999).
9. J.S. Blakemore, J. Appl. Phys. **53**, R123 (1982).
10. I. Vurgaftman, J.R. Meyer, and L.R. Ram-Mohan, J. Appl. Phys. **89**, 5815 (2001).
11. D.R. Lide (ed.), *Handbook of Chemistry and Physics, 72nd Ed.* (Boca Rotan: CRC Press, 1991).
12. W. Jost, J. Chem. Phys. **1**, 466 (1933).
13. G.D. Watkins, in *Radiation Damage in Semiconductors*, ed. P. Baruch, p97 (Paris:Dunod, 1965).
14. J.C. Bourgoin and J.W. Corbett, Phys. Lett. A **38**, 135 (1972).
15. J.C. Bourgoin, H.J. Bardeleben, D. Stiévenard, J. Appl. Phys. **64**, R65 (1988).

DISTRIBUTION

(to be distributed electronically)

1	MS0899	Technical Library	9536	(electronic copy)
1	MS1179	L. J. Lorence	1341	(ljloren@sandia.gov)
1	MS1056	W. R. Wampler	1111	(wrwampl@sandia.gov)
1	MS1323	E. R. Keiter	1445	(erkeite@sandia.gov)
1	MS1315	J. S. Nelson	1131	(jsnelso@sandia.gov)
1	MS1189	T. R. Mattsson	1641	(trmatts@sandia.gov)
1	MS0457	R. A. Paulsen	2211	(rapauls@sandia.gov)
1	MS1415	A. F. Wright	1131	(afwrigh@sandia.gov)